OPEN ACCESS Freely available online

PLOS | COMPUTATIONAL BIOLOGY

Pathway Thermodynamics Highlights Kinetic Obstacles in Central Metabolism

Elad Noor[1☯], Arren Bar-Even[1☯], Avi Flamholz[1,2], Ed Reznik[3], Wolfram Liebermeister[4], Ron Milo[1]*

1 Department of Plant Sciences, The Weizmann Institute of Science, Rehovot, Israel, **2** Department of Molecular and Cellular Biology, University of California, Berkely, Berkely, California, United States of America, **3** Computational Biology Program, Memorial Sloan-Kettering Cancer Center, New York, New York, United States of America, **4** Institut für Biochemie, Charité-Universitätsmedizin Berlin, Berlin, Germany

Abstract

In metabolism research, thermodynamics is usually used to determine the directionality of a reaction or the feasibility of a pathway. However, the relationship between thermodynamic potentials and fluxes is not limited to questions of directionality: thermodynamics also affects the kinetics of reactions through the flux-force relationship, which states that the logarithm of the ratio between the forward and reverse fluxes is directly proportional to the change in Gibbs energy due to a reaction (Δ_rG'). Accordingly, if an enzyme catalyzes a reaction with a Δ_rG' of -5.7 kJ/mol then the forward flux will be roughly ten times the reverse flux. As Δ_rG' approaches equilibrium ($\Delta_rG' = 0$ kJ/mol), exponentially more enzyme counterproductively catalyzes the reverse reaction, reducing the net rate at which the reaction proceeds. Thus, the enzyme level required to achieve a given flux increases dramatically near equilibrium. Here, we develop a framework for quantifying the degree to which pathways suffer these thermodynamic limitations on flux. For each pathway, we calculate a single thermodynamically-derived metric (the Max-min Driving Force, MDF), which enables objective ranking of pathways by the degree to which their flux is constrained by low thermodynamic driving force. Our framework accounts for the effect of pH, ionic strength and metabolite concentration ranges and allows us to quantify how alterations to the pathway structure affect the pathway's thermodynamics. Applying this methodology to pathways of central metabolism sheds light on some of their features, including metabolic bypasses (*e.g.*, fermentation pathways bypassing substrate-level phosphorylation), substrate channeling (*e.g.*, of oxaloacetate from malate dehydrogenase to citrate synthase), and use of alternative cofactors (*e.g.*, quinone as an electron acceptor instead of NAD). The methods presented here place another arrow in metabolic engineers' quiver, providing a simple means of evaluating the thermodynamic and kinetic quality of different pathway chemistries that produce the same molecules.

Citation: Noor E, Bar-Even A, Flamholz A, Reznik E, Liebermeister W, et al. (2014) Pathway Thermodynamics Highlights Kinetic Obstacles in Central Metabolism. PLoS Comput Biol 10(2): e1003483. doi:10.1371/journal.pcbi.1003483

Editor: Daniel A. Beard, University of Michigan, United States of America

Received June 18, 2013; **Accepted** January 8, 2014; **Published** February 20, 2014

Funding: RM is the incumbent of the Anna and Maurice Boukstein Career Development Chair in Perpetuity. RM is supported by the European Research Council (260392 – SYMPAC), Israel Science Foundation (Grant 750/09), the Ministry of Science (grant 711582), Helmsley Charitable Foundation, The Larson Charitable Foundation, Estate of David Arthur Barton, Anthony Stalbow Charitable Trust & Stella Gelerman, Canada. WL is supported by the German Research Foundation (LI 1676/2-1). The funders had no role in study design, data collection and analysis, decision to publish, or preparation of the manuscript.

Competing Interests: The authors have declared that no competing interests exist.

* E-mail: ron.milo@weizmann.ac.il

☯ These authors contributed equally to this work.

Introduction

A primary scientific goal of metabolic research is to develop an understanding of the evolutionary, chemical and physical forces that shape the structure of cellular metabolism. Specifically, to what extent are present-day metabolic pathways the result of evolutionary optimization rather than fossilized accidents? In recent years various aspects of central metabolism have been explained on the basis of specific selection pressures and constraints imposed during evolution [1,2,3,4,5,6,7,8,9,10,11,12,13]. Among the various constraints that shape the structure of metabolic pathways, thermodynamics features prominently, linking fundamental physical properties to pathway architecture [1,9,10,11,14,15,16]. Thermodynamic profiling also plays a central role in synthetic pathway design by identifying the most promising candidate pathways and discarding infeasible ones [14,17,18,19,20,21].

Thermodynamic analysis is typically applied to determine whether a reaction direction or pathway is feasible in physiological conditions [9,22]. Although not widely appreciated, thermodynamic potentials also constrain the kinetics of biochemical reactions and pathways [13,23,24,25]. Specifically, the Gibbs energy dissipated by a reaction, Δ_rG', affects the net reaction rate through the flux-force relationship [23]: $\Delta_rG' = -RT\ln(J^+/J^-)$, R being the gas constant, T the temperature, J^+ the forward flux and J^- the backward flux. Consequently, an enzyme catalyzing a reaction that is far from equilibrium ($\Delta_rG' << 0$) carries almost no backwards flux (Figure 1a) while an enzyme catalyzing a near-equilibrium reaction ($\Delta_rG' \sim 0$) "wastes" many enzyme units catalyzing substantial flux through the reverse reaction. According to the flux-force relationship, as a reaction shifts towards equilibrium we would see an exponential increase in the number of enzyme units required to catalyze a single unit of flux. For example, a Δ_rG' of -7.3 kJ/mol implies that about 5% of the enzymatic flux is in the reverse direction. Alternatively, a rather close-to-equilibrium Δ_rG' of -1 kJ/mol implies that about 40% of the enzymatic flux is in the reverse direction and the reaction rate

Author Summary

Given data about enzyme kinetics and reaction thermodynamics, traditional metabolic control analysis (MCA) can pinpoint the enzymes whose expression will have the largest effect on steady-state flux through the pathway. These analyses can aid experimentalists in tuning enzyme expression levels along a metabolic pathway. In this work, we offer a framework that is complementary to MCA. Rather than focusing on the relationship between enzyme levels and pathway flux, we examine a pathway's stoichiometry and thermodynamics and ask whether it is likely to support high flux in cellular conditions. Our framework calculates a single thermodynamically-derived metric (the MDF) for each pathway, which is convenient for selecting the promising pathways from a large collection. This approach has several advantages. First, enzyme kinetic properties are laborious to measure and differ between organisms and isozymes, but no kinetic data is required to calculate the MDF. Second, as our framework accounts for pH, ionic strength and allowed concentration ranges, it is simple to model the effect of these parameters on the MDF. Finally, as it can be difficult to control the exact expression level of enzymes within cells, the MDF helps identify alternative pathways that are less sensitive to the levels of their constituent enzymes.

is only ~20% of the rate that would be achieved if all enzyme units catalyzed the forward reaction.

Metabolic Control Analysis (MCA) is commonly used to describe the control that enzymes exert on metabolic fluxes [26,27,28,29,30]. This methodology starts with a given steady-state and mathematically describes how changes in enzyme abundance affect the pathway flux. Application of MCA requires enzyme kinetic properties which are laborious to measure and differ between organisms and isozymes. Here, we describe a complementary approach that requires no kinetic data and is not dependent on a particular initial steady state. We aim to identify pathways that, due to their thermodynamics, likely require higher enzyme levels to catalyze a unit of flux. Further, we pinpoint the particular pathway reactions responsible for these thermodynamic limitations. The flux-force relationship is instrumental in these analyses as it expresses a relationship between the Gibbs energy dissipated during a reaction ($\Delta_r G'$) and the amount of enzyme required to sustain a particular flux through that reaction. Therefore, the protein burden imposed by a pathway is directly related to the thermodynamic landscape of that pathway.

We develop a quantitative framework to analyze the thermodynamic landscape of metabolic pathways. Our framework identifies those reactions within a pathway whose rates are constrained by low thermodynamic driving force. These enzymes will constrain the activity of the pathway unless they are present at high concentrations or are much faster-than-average catalysts [31]. Using this methodology it is straightforward to compare different pathways that achieve similar metabolic goals (unlike MCA, which assumes a particular steady-state for each pathway, making comparison difficult). To demonstrate our method, we apply it to pathways of central metabolism, including fermentation pathways (e.g., Embden-Meyerhof-Parnas (EMP) glycolysis) and oxidative pathways (e.g., TCA cycle). We compare various alternative pathways by their thermodynamic landscapes and identify the reactions supported by a low thermodynamic driving force and, hence, requiring a high enzyme expression level.

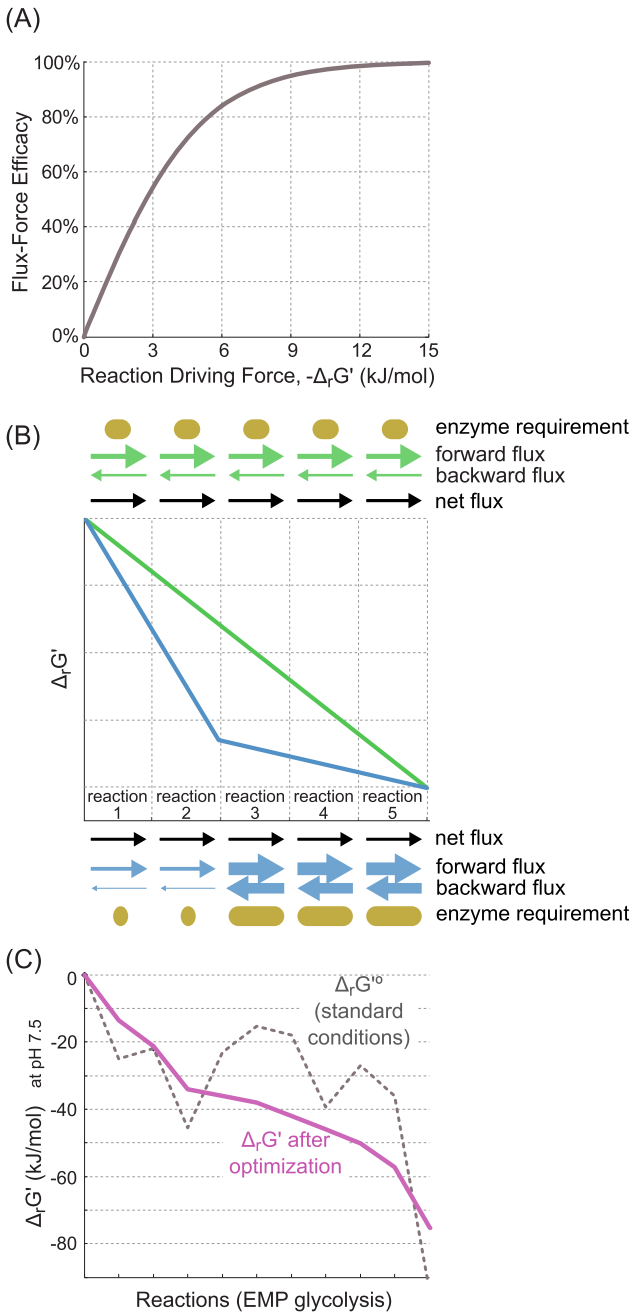

Figure 1. The Flux-Force Efficacy and Minimum Optimized Driving-Force (MDF). (A) A functional relationship between the reaction driving force ($-\Delta_r G'$) and its Flux-Force Efficacy, as described in detail in the Methods section. (B) Schematic comparison between two pathways. Each pathway starts and ends with the same compounds, employs five enzymes and carries the same net flux. The kinetic parameters of all enzymes in both pathways, as well as enzyme and metabolite concentrations, are assumed to be identical. (C) Energetic profile of Embden-Meyerhof-Parnas glycolysis. Dashed black line corresponds to $\Delta_r G'^{o}$ values (metabolite concentrations of 1 M) of pathway reactions at pH 7.5. Red line corresponds to $\Delta_r G'$ values of pathway reactions after an optimization procedure that maximizes the driving force of the reactions having the lowest driving forces, as described in the Methods section.
doi:10.1371/journal.pcbi.1003483.g001

Methods

Thermodynamic parameters

We used the Component Contribution method [32] for estimating the standard Gibbs energies of reactions, $\Delta_r G'^o$ (reactant concentrations of 1 M). This method produces a consistent set of $\Delta_r G'^o$ values by integrating three sources of information in decreasing priority: (1) ~200 Gibbs energies of formation ($\Delta_f G^o$) collected and published by Alberty [33,34]; (2) apparent equilibrium constants (K′) available in the NIST database of enzyme-catalyzed reactions [35,36]; and (3) the pseudoisomeric group contribution method as described in detail in ref. [22]. All $\Delta_r G'^o$ values were transformed to a pH of 7.5 and an ionic strength of 0.2 M [22], representing typical cellular conditions [37]. We use these conditions in all analyses presented in this paper, unless stated otherwise.

Driving force and pathway feasibility

The Gibbs energy dissipated by a reaction can be calculated from the standard Gibbs energy of the reaction ($\Delta_r G'^o$) and the reactant concentrations. It is given by $\Delta_r G' = \Delta_r G'^o + RT \cdot ln(Q)$, where Q is the reaction quotient (also known as the mass action ratio). Because of its more intuitive sign we will often refer to a reaction's *Driving Force*, defined as $-\Delta_r G'$ [38].

When analyzing pathways containing multiple reactions, it is convenient to use matrix notation [39]. We define $\mathbf{S}$ as the stoichiometric matrix, with rows corresponding to compounds and columns to reactions; *i.e.*, S_{ij} is the stoichiometric coefficient of compound i in reaction j (positive for products and negative for substrates). $\boldsymbol{G^o}$ *denotes* a column vector of reaction energies, *i.e.*, G^o_j is the standard change in Gibbs energy ($\Delta_r G'^o$) of reaction j. Finally, let $\boldsymbol{x}$ be the column vector of the log-concentrations, so that x_i is the natural logarithm of the concentration of compound i in molar units. Then the vector of reaction driving forces ($-\boldsymbol{\Delta_r G'}$) is given by $-(\boldsymbol{G^o} + RT \cdot \mathbf{S}^{\mathrm{T}} \cdot \boldsymbol{x})$.

We use a convention where all reactions in $\mathbf{S}$ are written such that the forward direction is the direction of the net flux in the pathway, and the stoichiometric coefficients represent the actual molecularities in the enzyme's reaction center [38] (*i.e.*, the number of reactant molecular entities that are involved in the 'microscopic chemical event' constituting an elementary reaction). This convention obviates the situation existing in more general stoichiometric models [40], where scaling the flux of a reaction by a scalar and dividing the stoichiometric coefficients of that reaction by the same factor results in an equivalent system. Using the actual molecularities is vital for our analysis, as the flux-force relationship cannot accept an arbitrary definition of stoichiometry.

Considering $\boldsymbol{G^o}$ to be constant and allowing $\boldsymbol{x}$ to vary, a pathway is feasible if and only if there is at least one solution to the linear system defined by the constraints $\ln(C_{min}) \le \boldsymbol{x} \le \ln(C_{max})$ and $-\boldsymbol{\Delta_r G'} > 0$; *i.e.*, there must exist a set of metabolite concentrations within the predefined range (C_{min} to C_{max}) such that all reactions have a positive driving force. The concentration bounds (C_{min} and C_{max}) may be the same for all compounds or can be defined individually.

Even if a pathway is composed of thermodynamically-feasible reactions, the pathway may be thermodynamically infeasible as a whole. That is, no solution for $\boldsymbol{x}$ exists within the chosen concentration range such that $-\boldsymbol{\Delta_r G'} > 0$ and so the pathway reactions cannot all be made feasible simultaneously [41].

Flux-Force Efficacy and Max-min Driving Force (MDF)

As described in the Introduction, the driving force of a reaction constrains its rate, with near-equilibrium reactions requiring exponentially more enzyme to sustain the same rate as reactions far from equilibrium. We define the *Flux-Force Efficacy* – a unitless measure between 0 and 1 – as the ratio between the net flux ($J^+ - J^-$) and the total flux ($J^+ + J^-$), which – according to the flux-force relationship – is related to the change in Gibbs free energy by $\frac{J^+ - J^-}{J^+ + J^-} = \frac{e^{-\frac{\Delta_r G'}{RT}} - 1}{e^{-\frac{\Delta_r G'}{RT}} + 1}$. Hence, the higher the driving force of a reaction, the higher its *Flux-Force Efficacy*.

Because of this interdependence between thermodynamic potentials and flux, pathways operating near equilibrium will incur a kinetic penalty due to backwards flux. We therefore attempt to quantify a pathway's tendency to operate near-equilibrium. We seek a set of reactant concentrations that will maximize the driving forces of all reactions in the pathway. To achieve this, we use the minimum over all reaction driving forces ($-\Delta_r G'$ values of pathway reactions) as an optimization goal and maximize it – within metabolite concentration bounds – using linear programming. This can be formalized as a linear problem:

$$\begin{aligned} \text{Given} \quad & \mathbf{S}, \mathbf{G}^\circ, RT, C_{\min}, C_{\max} \\ \underset{\mathbf{x},B}{\text{Maximize}} \quad & B \\ \text{Subject to} \quad & -(\mathbf{G}^\circ + RT \cdot \mathbf{S}^T \cdot \mathbf{x}) \ge B \\ & \ln(C_{\min}) \le \mathbf{x} \le \ln(C_{\max}) \end{aligned}$$

where B represents a tight lower bound (*i.e.*, the minimum) on the driving force of all reactions. Maximizing B yields a solution where all reactions are as far from equilibrium as possible given the defined concentration ranges. The maximal value of B is denoted as the ***M**ax-min **D**riving-**F**orce* (MDF) of the pathway and is measured in units of kJ/mol [42].

If a pathway has an MDF of 7.3 kJ/mol then a set of metabolite concentrations exists, within the pre-defined concentration range, such that all pathway reactions dissipate at least 7.3 kJ/mol. A $\Delta_r G' = -7.3$ kJ/mol corresponds to a J^+/J^- ratio of $\exp(7.3/RT) = 19$, which in turn suggest that 95% of the overall flux is in the forward direction and $95/19 = 5\%$ is in the backward direction. Therefore, the *Flux-Force Efficacy* is $95 - 5 = 90\%$ ($\frac{e^{-\frac{7.3}{RT}} - 1}{e^{-\frac{7.3'}{RT}} + 1} = 0.9$). Since the MDF is a tight bound, it is impossible to find a set of concentrations within the specified range for which all reaction driving forces are larger than, say, 7.4 kJ/mol. Notably, the MDF solution is also equivalent to minimizing the *total* enzyme mass in a linear pathway, assuming that all enzymes have the same specific activities (see Text S1 for a mathematical proof).

Reaction and Metabolite Shadow Prices

In order to quantify the extent to which a reaction or a metabolite affects the value of the MDF, we use the concept of shadow prices [42,43]. Every primal linear optimization problem has a complementary dual problem. The variables of the dual problem – called shadow prices – quantify how much the value of the primal objective – *i.e.*, the MDF – will increase when a single constraint is relaxed by a unit amount. There are three types of constraints in the MDF linear problem: the lower bound (B) of the reaction driving forces ($-\boldsymbol{G^o} - RT \cdot \mathbf{S}^{\mathrm{T}} \cdot \boldsymbol{x} \ge B$), the upper bound of metabolite concentrations ($\boldsymbol{x} \le \ln(C_{max})$), and the lower bound of metabolite concentrations ($\ln(C_{min}) \le \boldsymbol{x}$). We therefore define the *Reaction Shadow Price* as the shadow price associated with the constraint on the driving force of that reaction, representing how much a change in $\boldsymbol{G^o}$ will affect the MDF. The *Metabolite*

Shadow Price is the maximum of the absolute values of the two shadow prices associated with the constraints (lower and upper bound) on that metabolite's concentration.

The shadow prices are the solution for the variables of the dual problem $\mathbf{w}$, $\mathbf{u_{max}}$, $\mathbf{u_{min}}$:

$$\begin{array}{cc} \text{Given} & \mathbf{S},\mathbf{G}^{\circ},RT,C_{\min},C_{\max} \\ \underset{\mathbf{w},\mathbf{u_{max}},\mathbf{u_{min}}\geq 0}{\text{Minimize}} & -\mathbf{G}^{\circ}\mathbf{w}+C_{\max}\mathbf{u_{max}}-C_{\min}\mathbf{u_{min}} \\ \text{Subjectto} & \mathbf{S}\cdot\mathbf{w}+\mathbf{u_{max}}-\mathbf{u_{min}}=0 \\ & \sum_j \mathbf{w_j}=1 \end{array}$$

According to the definitions above, $\mathbf{w}$ are the *reaction* shadow prices and $\max(|\mathbf{u_{max}}|, |\mathbf{u_{min}}|)$ are the *metabolite* shadow prices. See Text S1 for a full derivation of the dual problem.

The shadow prices represent a scaling between a change in the constraint and the resulting change in the MDF. For example, a reaction shadow price of 0.25 indicates that a 4 kJ/mol decrease in $\Delta_r G'^{o}$ would increase the pathway MDF by 1 kJ/mol (assuming that this reaction still limits the pathway MDF). Similarly, a metabolite shadow price of 0.5, associated with the upper bound constraint, implies that raising the upper bound concentration of this metabolite by 10 fold will result in the MDF increasing by $0.5*RT\ln(10)\approx 3$ kJ/mol. Shadow prices are 0 for reactions whose $\Delta_r G'^{o}$ does not constrain the MDF, and likewise for metabolites whose concentrations do not constrain the MDF.

Metabolite concentration range

Throughout our analyses we used metabolite concentration bounds characteristic of cellular physiology, a lower bound $C_{min} = 1$ μM and an upper bound $C_{max} = 10$ mM [9,44,45]. An exception was made for cofactors, whose concentrations were fixed to those characteristic of *E. coli*'s cytoplasm. Cofactors participate in tens or even hundreds of reactions and so their concentrations are considerably more constrained by the endogenous metabolic network than common reaction intermediates [46]. Fixing the concentrations of cofactors allows us to encode these constraints imposed by the wider metabolic network on individual pathways. Wherever possible, we constrained the cofactor ratios rather than their absolute concentrations, since the ratios are more conserved in many cases. The co-factor constraints we use are as follows: [ATP]/[ADP] = 10 [45,47,48,49], [ADP]/[AMP] = 1 [45,49], [NADH]/[NAD^+] = 0.1 [45,50], [NADPH]/[$NADP^+$] = 10 [45, 51], [$Ferredoxin_{reduced}$]/[$Ferredoxin_{oxidized}$] = 1 (corresponds to a reduction potential of −400 mV [52]), [orthophosphate] = 10 mM [53,54,55], [pyrophosphate] = 1 mM [56,57], [CoA] = 1 mM [45], [CO_2(aq)] = 10 μM (ambient conditions).

Connection between thermodynamic driving forces and Metabolic Control Analysis

Enzyme abundances control the steady-state fluxes within a pathway [26,27,28,29,30]. When an enzyme is upregulated, the rate of the reaction it catalyzes increases instantaneously, but the rates of other reactions in the pathway do not change at first. This state, however, cannot be maintained for long as the concentration of the enzyme's substrates decrease, while its products accumulate. Therefore, other reactions in the pathway are affected, and eventually, after the system settles in a new steady state, all fluxes might be altered. The term "control" describes such indirect, global effects.

Potentially, all enzymes exert control on all fluxes within the pathway, but to different extents. Metabolic Control Analysis describes this control mathematically: if we consider small changes to a given steady-state, the effect of an enzyme's abundance on the pathway flux, can be quantified by the scaled flux control coefficient [26,58]:

$$C_{v_i}^{J}=\frac{E_i}{J}\frac{\partial J}{\partial E_i}$$

where J is the steady-state flux, v_i is the rate of reaction i and E_i is the abundance of the enzyme catalyzing reaction i. In the general case, control coefficients depend on the pathway structure, enzymatic parameters, and allosteric regulation. Since all control coefficients for a flux J always sum to 1 [58,59], control can only be redistributed among the different pathway enzymes.

The flux control coefficients are related to the thermodynamic driving forces, as derived in Text S1 and was shown in ref. [26]. This relationship is easily derived for linear pathways whose enzymes follow the reversible Michaelis-Menten rate laws [26,60,61]. In Text S1, we derive the relationship for two specific cases: (1) all enzymes are completely substrate (but not product) saturated. Importantly, because all enzymes are essentially reversible, the rates of all reactions are sensitive to the concentrations of the substrates and products, even if all enzymes are substrate saturated. A full analysis of this case is given ref. [61]; (2) the substrates and products of all enzymes are well below their K_M (enzymes operate in the linear regime). We show that in both cases the control coefficients are completely determined by reaction driving forces, such that the two are always correlated: the higher the driving force of a reaction, the higher the control it exerts on the pathway flux. Specifically, reactions with low driving forces have very low control coefficients.

For the first case – all enzymes are substrate-saturated – we find that $C_{v_i}^{J}=\alpha\left(e^{\frac{-\Delta_r G_i'}{RT}}-1\right)$.

For the second case – when all enzymes are substrate and product sub-saturated – we find that: $C_{v_i}^{J}=\alpha\left(e^{\frac{-\Delta_r G_i'}{RT}}-1\right)\left(\Pi_{m=1}^{i}e^{\frac{-\Delta_r G_m'}{RT}}\right)^{-1}$, in agreement with the derivation of [26].

In both cases the scaling factor α is identical for all reactions and is determined by $\Sigma_i C_{v_i}^{J}=1$.

Software

The software for all the analyses presented in this paper is open source (MIT license) and stored in an online repository (https://code.google.com/p/milo-lab/). We use IBM's ILOG CPLEX Optimization Studio 12.5 to solve the MDF primal and dual problems. The code which predicts the standard Gibbs energies [32] also depends on OpenBabel (http://openbabel.org) [62], Calculator Plugins from Marvin (version 5.10.1) by ChemAxon, and the KEGG database (http://www.genome.jp/kegg/) [63].

Results

The Flux-Force Efficacy and the Max-min Driving-Force (MDF)

The kinetics of a reaction can be linked to three main factors: (1) maximal velocities and saturation levels, related to the enzyme kinetic parameters and to the concentrations of substrates and products; (2) enzyme abundances and (3) reverse flux though reactions [13]. Thermodynamics determines this last factor through the flux-force relationship: the reaction driving force (equivalent to the minus of the reaction change in Gibbs energy,

i.e., $-\Delta_r G'$) equals $RT\ln(J^+/J^-)$, as presented above. For low enough driving forces (roughly 3 kJ/mol or less) the effect of $\Delta_r G'$ on the reaction flux is similar to that of k_{cat} (or V_{MAX}) in the sense that a fold change in either of them will change the reaction rate by the same fold change. The dependence of the reaction rate on $-\Delta_r G'$ decreases as $-\Delta_r G'$ increases above ~3 kJ/mol. When $-\Delta_r G'$ exceeds 10 kJ/mol, the reaction rate is effectively insensitive to thermodynamic effects, reflecting the fact that there is negligible flux in the reverse direction.

To address the effect of driving force on reaction flux more systematically, we define the Flux-Force Efficacy as the ratio between reaction net flux and total flux, $\frac{J^+ - J^-}{J^+ + J^-}$ (Methods). The Flux-Force Efficacy can be interpreted as the ratio between the actual reaction rate and the rate expected if backward flux was insignificant (assuming maximal velocities, saturation levels and enzyme concentrations are kept constant). Figure 1A shows how this ratio scales with the reaction driving force.

We use the term "efficacy", instead of "efficiency", to distinguish between Flux-Force Efficacy and thermodynamic efficiency, as the two are antagonistic. For example, a reaction operating close to equilibrium is often considered to be thermodynamically efficient since it dissipates almost no Gibbs energy. Yet, such a reaction is characterized by a low Flux-Force Efficacy as $J^+ \approx J^-$. In contrast, a reaction with a high Flux-Force Efficacy, characterized by $J^+ >> J^-$, is thermodynamically inefficient, dissipating a considerable amount of Gibbs energy.

For a fixed enzyme level, a high Flux-Force Efficacy implies a high net reaction rate, as backward flux is negligible. On the other hand, a low Flux-Force Efficacy indicates considerable backward flux, leading to a decreased reaction rate. In a complementary manner, we can use this relationship to estimate the amount of enzyme required to sustain a particular flux through the reaction [13]. Figure 1B demonstrates this effect schematically using the energetic profiles of two putative pathways. Both pathways start and end with the same compounds, employ five enzymes and carry the same net flux. The kinetic parameters of all enzymes in both pathways, as well as enzyme and metabolite concentrations, are assumed to be identical. All reactions in the green pathway have the same, moderate driving force, which translates to a small backward flux. Hence, a small amount of each enzyme suffices. In the blue pathway, the driving force of the first two reactions is large while the last three reactions are near equilibrium. These final three reactions, therefore, require a lot more catalyst in order to sustain the same flux as the first two reactions in the blue pathway.

When analyzing an entire pathway, it is essential to consider the interplay between the driving forces of all participating reactions: varying the concentration of a given metabolite can modulate the driving force of multiple reactions. We developed a method for finding metabolite concentrations – within an allowed range, see Methods – that maximize the driving force, and hence the Flux-Force Efficacy, of pathway reactions. Specifically, our computational tool uses the minimum over all reaction driving forces as an optimization function and maximizes it (Methods). This minimum, representing the smallest driving force among all pathway reactions, is defined as the **M**ax-min **D**riving-**F**orce (MDF).

Figure 1C illustrates the application of the optimization approach to EMP glycolysis. The grey dashed line represents the $\Delta_r G'^o$ values of the different pathway reactions, while the magenta line represents the $\Delta_r G'$ values for each of the reactions after optimizing reactant concentrations to maximize the MDF. After this optimization, all reactions in the pathway have a positive driving force (*i.e.*, a negative slope) and so it is clear that the EMP pathway is thermodynamically feasible.

Presuming the $\Delta_r G'^o$ values used are accurate and that our concentration bounds reflect cellular concentrations, pathways are thermodynamically feasible if and only if they have a positive MDF. Moreover, the value of the MDF indicates the degree to which a pathway is expected to be kinetically constrained by backward flux. A pathway with a high MDF can achieve a steady-state with very low backward flux as all of its constituent reactions can achieve high driving forces simultaneously. On the other hand, a pathway characterized by a low MDF contains reactions that are expected to have low driving force in physiological conditions. Due to the flux-force relationship, these reactions must either sustain low flux or be catalyzed by an abundant enzyme. For example, the green pathway shown in Figure 1B operates at high MDF which results in a high pathway flux and/or a low enzyme requirement. On the other hand, the blue pathway operates at low MDF, containing near-equilibrium reactions which reduce pathway flux and/or require higher enzyme levels.

The shadow prices determine whether a specific reaction or metabolite constrains the pathway MDF, as described in detail in the Methods section. A decrease in the $\Delta_r G'^o$ value of a reaction with a positive shadow price would lead to an increase in the MDF. Similarly, if the concentration of a metabolite with a positive shadow price is permitted to violate the allowed concentration range (becomes too high or too low), the MDF increases (Methods).

According to our model, enzymes catalyzing reactions with positive shadow prices are expected to be present at higher concentrations or have higher-than-average k_{cat} values. While it is tempting to test this hypothesis systematically, it is, unfortunately, very challenging using available experimental data. Specifically, the MDF analysis requires that the magnitudes of all fluxes are precisely determined (taking into account that the flux through enzymes participating in the same pathway might differ due to an overlap with other metabolic routes). However, even for the relatively simple case of *E. coli*'s central metabolism, flux and metabolite concentration measurements from different groups vary significantly, even when performed under similar conditions (*e.g.*, [64,65]). In addition, proteomic measurements related to lowly-expressed proteins are still quite noisy. Finally, most kinetic parameters reported in the literature were measured *in vitro*, which can differ considerably from those experienced *in vivo* [66,67]. These issues limit our ability to perform a comprehensive systematic analysis of the relationship between the thermodynamic parameters, the measured k_{cat} values and enzyme levels. Our current contribution suggests specific predictions to be tested when the needed experimental technologies mature.

In the sections below we demonstrate our methodology by applying it to well-known central metabolic pathways. Our analysis, although not systematic, provides several examples of thermodynamic properties affecting pathway flux and suggests thermodynamic based explanations for key biochemical phenomena.

Malate dehydrogenase constrains the Max-min Driving-Force of the TCA pathway

In most organisms, the TCA cycle is the pathway responsible for the catabolic oxidation of organic compounds to CO_2 (Figure 2A). Figure 2B presents the MDF of the TCA cycle (solid blue line) as a function of pH. We chose to vary pH, rather than other factors that affect the MDF, because cellular pH can differ considerably between organisms [37] and because the thermodynamics of many biochemical reactions producing or consuming protons is greatly

affected by changes in pH. Figure 2B shows that the TCA cycle has a low MDF. In fact, it seems infeasible at pH≤7, which contradicts the observation that numerous organisms operate the TCA cycle at low cytosolic pH values [37]. To understand this puzzling finding, we asked which reaction(s) are responsible for constraining the pathway's MDF – *i.e.*, which reactions have a positive shadow price. We find that, at non-alkaline conditions, the only reaction with a positive shadow price is malate dehydrogenase. The oxidation of malate to oxaloacetate using NAD as an electron acceptor (marked in red in Figure 2A) is characterized by a large positive $\Delta_r G'^o$ (>30 kJ/mol at pH≤7). How, then, are cells able to sustain high flux through the TCA cycle? The MDF framework enables us to suggest solutions for this apparent paradox.

First, a high turnover number can compensate for operating at a low MDF: if the maximal activity of an enzyme is high enough, it will be able to operate sufficiently fast even at a low Flux-Force Efficacy. For example, an enzyme having a k_{cat} of 100 s^{-1} and catalyzing a reaction with a driving force of only 0.3 kJ/mol (Flux-Force Efficacy ~6%) is equivalent to an enzyme having a k_{cat} of 10 s^{-1} (the average k_{cat} [31]) but catalyzing a reaction with a driving of 3 kJ/mol (Flux-Force Efficacy >50%). Thus, the high turnover number of malate dehydrogenase (well above 1000 s^{-1} [31]) might have evolved to compensate for its low driving force. However, this compensation effect does not answer how the cycle can carry flux at pH≤7, when malate oxidation is expected to become infeasible.

Another possible explanation is that the concentration of oxaloacetate – having a positive shadow price (Figure 2A) – is lower than 1 μM, the lower-bound concentration assumed in our analysis. As oxaloacetate is an unstable compound [68], it is tempting to suggest that it is indeed found at a sub-micromolar concentration *in-vivo*. As shown in Figure 2B, allowing oxaloacetate concentrations beneath 1 μM increases the pathway's MDF and the pH range in which it is thermodynamically feasible. However, keeping the concentration of oxaloacetate so low might be deleterious, as it would limit the rate of reactions which utilize this metabolite, *e.g.*, citrate synthase, aspartate transaminase and PEP carboxykinase. In fact, the relatively high affinity of citrate synthase towards oxaloacetate – K_M being on the order of 1 μM [31,69] – can be interpreted as representing an adaptation towards a low oxaloacetate concentration.

A further possibility, also supported by experimental studies, is that oxaloacetate is channeled between malate dehydrogenase and citrate synthase [70,71,72,73]. If channeling indeed takes place, the cellular concentration of oxaloacetate can be extremely low without compromising the rate of the enzymes utilizing it. From a thermodynamic point of view, malate dehydrogenase and citrate synthase can then be treated as a single reaction [9,74]. This unified reaction does not represent any thermodynamic difficulty as its $\Delta_r G'^o$ is lower than −20 kJ/mol. As shown in Figure 2B, such a scenario increases the pathway MDF and makes it feasible in any physiological pH. Following the logic that substrate channeling can alleviate thermodynamic constraints, we expect that metabolites with positive shadow prices (*i.e.*, whose concentration constrains the pathway MDF) will have a higher propensity to be channeled between enzymes, therefore potentially guiding experimental efforts to such locations in search of evidence for substrate channeling. When high throughput methods for identifying channeling are developed, it will be possible to test this hypothesis systematically.

Another solution to this thermodynamic puzzle might be the use of electron acceptors with a higher reduction potential than that of NAD. For example, various organisms operate a malate:quinone oxidoreductase enzyme [75,76,77,78,79]. In many of these organisms, this enzyme replaces more common NAD-dependent enzymes as the major route of malate oxidation [76,77,78,79]. As shown in Figure 2B, using malate:quinone oxidoreductase enables the TCA cycle to operate at high MDF regardless of the cytoplasmatic pH. The downside of this approach is that less ATP can be produced via oxidative phosphorylation when using a quinone as an electron carrier instead of NAD.

Finally, it is important to note that the TCA cycle is not actually a cycle in many organisms and under various conditions (*e.g.*, [80]). Instead, it often operates in a forked-mode, where malate dehydrogenase catalyzes the favorable direction (*i.e.*, oxaloacetate reduction), eliminating the thermodynamic constraints due to malate oxidation. Remarkably, it was recently suggested that *E. coli* uses a forked TCA cycle even during aerobic growth, despite the low ATP yield associated with this mode [65].

Several natural alternatives to the TCA cycle are also known to support the complete oxidation of organic compounds to CO_2 [64,81]. The structures of these pathways are given in Figure S1. Figure 2C compares these metabolic alternatives on the basis of their MDF and ATP yield per glucose. ATP is assumed to be produced from substrate-level phosphorylation and from NAD(P)H through oxidative phosphorylation. The P/O ratio – measuring how many ATP molecules are produced per one oxygen atom being reduced – was taken to be 1.5, the representative value for *E. coli* [82]. Figure 2C suggests that the TCA cycle represents a combination of high ATP yield and high MDF which is better than most of its counterparts – especially if assuming substrate channeling of oxaloacetate ('TCA channel') or the usage of quinone instead of NAD ('TCA MQO'). The oxidative pentose phosphate pathway ('OxPP'), while producing less ATP molecules than the TCA cycle, supports the highest MDF among all oxidative pathways.

Substrate-level phosphorylation constrains the Max-min Driving-Force of fermentation pathways

EMP glycolysis (Figure 3A) is the most investigated fermentation pathway [10]. Substrate-level phosphorylation – coupled to glyceraldehyde 3-phosphate oxidation – is the process responsible for *de novo* ATP synthesis in the pathway (the downstream pyruvate kinase only recoups the ATP invested at the beginning of the pathway) [10]. Nevertheless, some organisms bypass substrate-level phosphorylation altogether such that glyceraldehyde 3-phosphate is directly oxidized to glycerate 3-phosphate, without producing ATP (Figure 3B) [83,84]. Using the MDF methodology we can offer some insight as to why this may be.

Figure 3C displays the MDF of the EMP pathway – with and without substrate-level phosphorylation – as a function of cellular pH. While the EMP pathway has a very low MDF and seems to be infeasible at pH<6.5, the pathway variant which bypasses substrate-level phosphorylation is characterized by a far higher MDF. This suggests that organisms that do not depend on the degradation of organic compounds for energy conservation – like phototrophs or obligatory respiratory prokaryotes – can profit considerably by skipping substrate-level phosphorylation and operating at a much higher MDF, which can be translated into higher flux or, alternatively, to a lower protein investment required to sustain a given rate [13].

Notably, the trend shown in Figure 3C does not mean that the two substrate-level phosphorylation reactions (glyceraldehyde phosphate dehydrogenase and phosphoglycerate kinase) are the only ones that constrain the pathway MDF. The five reactions marked in red in Figure 3A are those with positive shadow price, showing that multiple reactions constrain the driving force of the

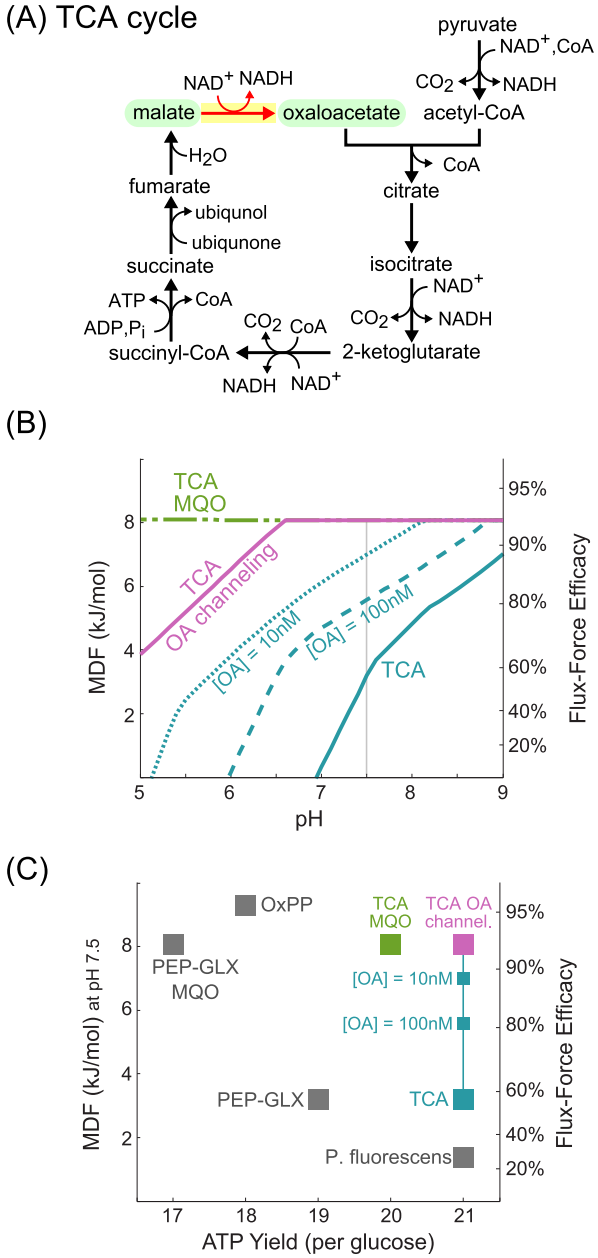

Figure 2. MDF analysis of oxidative pathways. (A) Structure of the TCA cycle. The reaction marked in red is the only one with a positive shadow price at pH 7.5. Non-cofactor metabolites shaded in green show positive shadow prices. (B) MDF as function of pH, as calculated for the TCA cycle and several of its similar variants. Solid cyan line: default metabolite concentration range used throughout this study (1 μM–10 mM). Dashed and dotted cyan lines: oxaloacetate concentration (marked as 'OA') is allowed to attain lower values, 100 nM and 10 nM, respectively. Solid magenta line: oxaloacetate is channeled ('channeling') between malate dehydrogenase and citrate synthase. Semi-dashed green line: quinone ('MQO') serves as the electron acceptor in malate oxidation, instead of NAD. The Flux-Force Efficacy axis, on the right, refers to the reactions that dissipate the smallest amount of Gibbs energy, and hence equal to the pathway MDF. The light grey line marks the values corresponding to pH 7.5, the pH used in (C). (C) The MDF and ATP yield per glucose of the different oxidative pathways. 'PEP-GLX' corresponds to the PEP-Glyoxylate pathway, which was found to operate in *E. coli* under glucose starvation [64]. '*P. fluorescens*' corresponds to the pathway used by *Pseudomonas fluorescens* under conditions of aluminum toxicity [81]. 'OxPP' corresponds to the oxidative pentose phosphate cycle, which can be used to fully oxidize sugars into CO_2, providing NADPH for cellular activity. Reducing power was assumed to be converted to ATP via oxidative phosphorylation, where NADH or a pair of reduced ferredoxins give rise to 1.5 ATP molecules and reduced ubiquinone produces one ATP molecule. The structures of all pathways are given in Figure S1.

doi:10.1371/journal.pcbi.1003483.g002

EMP pathway. In fact, if any reaction from fructose bisphosphate aldolase to phosphoglycerate mutase had a more favorable $\Delta_r G'^o$ value then the MDF of the entire pathway would increase.

Fructose bisphosphate is one of the two non-cofactor metabolites with a positive shadow prices (Figure 3A), and the only one whose concentration upper bound (10 mM) limits the pathway MDF (Methods). Interestingly, the concentration of fructose bisphosphate has been measured to be 15 mM [45], the only glycolytic metabolite whose concentration is higher than 10 mM. This 50% higher concentration adds ~1 kJ/mol to the driving force of the thermodynamically-constrained reactions, increasing their rather low Flux-Force Efficacies. This example demonstrates how the methodology presented here can be used to rationalize why certain compounds attain higher (or lower) concentrations than others in cells. This further suggests a systematic study of whether an energetic analysis, as the one outlined here, can predict metabolite concentrations on a large scale. However, the measurement of metabolite concentrations using current technologies remains quite noisy, as evident by the dramatic discrepancies between different quantification methods (*e.g.*, [46]). As measurement technology matures, the generality of the connection between the range of metabolite concentrations and the thermodynamically-constrained reactions could be evaluated systematically.

Several glycolytic variants are known to exist in nature and their structures and shown in Figure S2. Figure 3D plots the MDF (at pH 7.5) of each of these pathways against the number of ATP molecules it produces per glucose molecule metabolized. As shown in the figure, there is a clear tradeoff between the MDF and ATP yield, with high- MDF pathways conserving less energy as ATP than pathways with lower MDF. Specifically, the methylglyoxal pathway ('MGX') – converting dihydroxyacetone phosphate into the highly reactive compound methylglyoxal [85,86,87] – and the non-phosphorylative Entner-Doudoroff (ED) pathway ('EDNP') – used by hyperthermophilic archaea [84,88,89] – seem to be promising choices for fermenting glucose if ATP production is not important but a high glycolytic flux is required [13].

Within the general trend shown in Figure 3B, some pathways seem better than others. The non-phsophorylative ED pathway, the phosphoketolase pathway ('PKT') – using the pentose phosphate pathway and cleaving xylulose-phosphate to glyceraldehyde-phosphate and acetyl-phosphate [90,91] – and the pyruvate formate lyase pathway ('EMP PFL') – cleaving pyruvate to acetyl-CoA and formate and performing substrate-level phosphorylation on acetyl-phosphate – lie on the Pareto front [92], *i.e.*, no other pathway has both a higher MDF and a higher ATP yield. Notably, despite their prevalence in nature, neither the EMP nor the ED pathways are on the Pareto front, which suggests that thermodynamic properties alone are insufficient to explain the structure of central metabolism pathways, as we previously analyzed in detail (*e.g.*, [10]). Specifically, the phosphoketolase and pyruvate formate lyase pathways have higher MDF values than the EMP and ED pathways and yield at least as much ATP. However, it is known that other factors constrain the operation of these pathways in nature. The pyruvate formate lyase enzyme (EC 2.3.1.54) employs an oxygen-sensitive radical mechanism and so

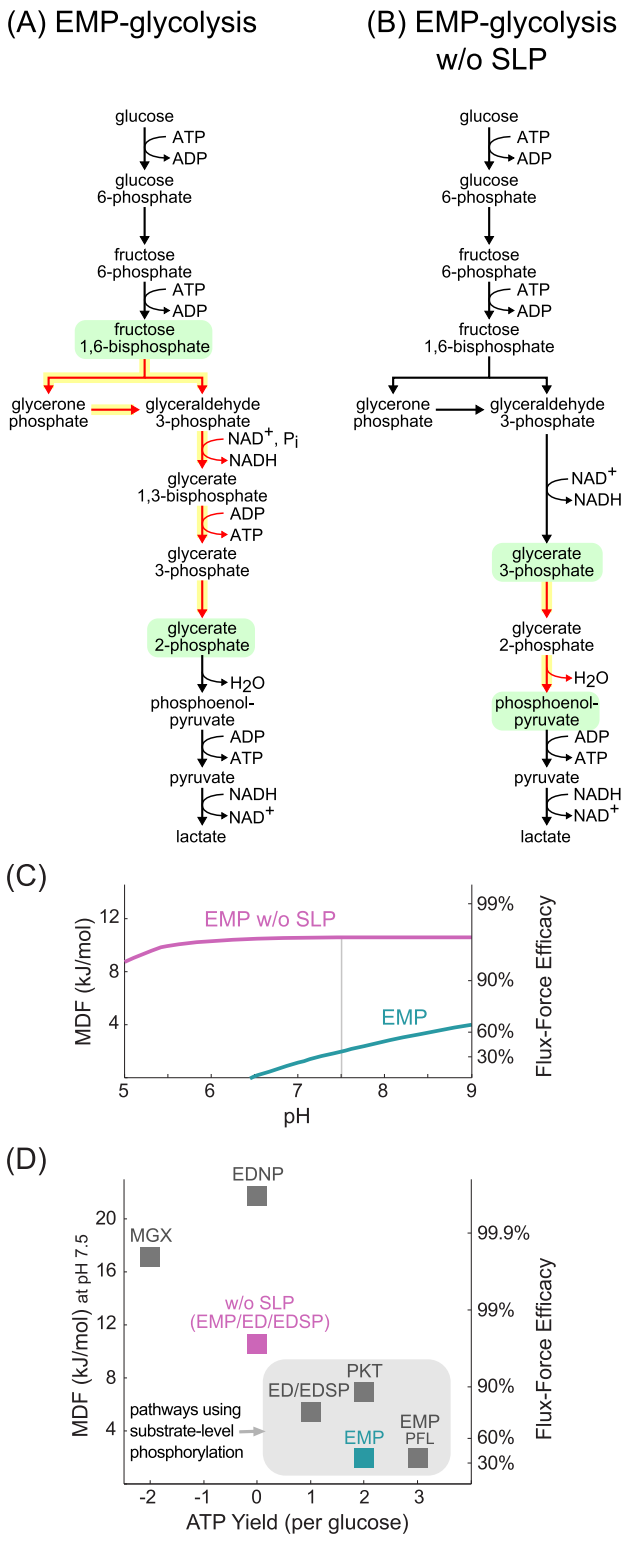

Figure 3. MDF analysis of fermentation pathways. (A) Structure of EMP-glycolysis. (B) Structure of an EMP pathway variant in which substrate-level phosphorylation is bypassed. The reactions marked in red are those with positive shadow prices at pH 7.5. Non-cofactor metabolites shaded in green show positive shadow prices. (C) MDF as function of pH, as calculated for the EMP pathway (cyan) and for an EMP pathway variant in which substrate-level phosphorylation is bypassed (magenta). 'SLP' corresponds to substrate-level phosphorylation. The Flux-Force Efficacy axis, on the right, refers to the reactions that dissipate the smallest amount of Gibbs energy, and hence equal to the pathway MDF. The light grey line marks the values corresponding to pH 7.5, the pH used in (D). (D) The MDF and ATP yield per glucose of the different fermentation pathways. 'ED' corresponds to the Entner-Doudoroff pathway. 'EDSP' represents the semi-phosphorylative ED pathway, known to operate in several hyperthermophilic archaea lineages [84,88,89]. 'EDNP' represents the non-phosphorylative ED pathway, also known to operate in hyperthermophilic archaea [84,88,89]. 'MGX' corresponds to a variant of the EMP pathway in which dihydroxyacetone phosphate is converted into the toxic compound methylglyoxal when the concentration of inorganic phosphate becomes limiting [85,86,87]. 'PKT' represents a pathway, suggested long ago [103], that uses the pentose phosphate pathway in conjunction with the enzyme phosphoketolase that cleaves xylulose-phosphate to glyceraldehyde-phosphate and acetyl-phosphate [90,91]. 'EMP PFL' corresponds to a variant of the EMP pathway that produces more ATP by using the enzyme pyruvate formate lyase and performing substrate-level phosphorylation on of acetyl-phosphate. The structures of all pathways are given in Figure S2.
doi:10.1371/journal.pcbi.1003483.g003

can only be used in anaerobic or microaerobic environments [93,94,95]. This limitation may explain why the EMP-PFL pathway is less abundant in nature than MDF analysis would lead us to expect.

Discussion

We introduce a quantitative framework for analyzing the thermodynamic profile of metabolic pathways and identifying reactions that limit metabolic flux within feasible pathways (*i.e.*, require high enzyme levels to sustain a specific rate). While near-equilibrium reactions can significantly increase the protein burden of a pathway, they may have certain advantages. For example, if the direction of a reaction must change quickly in response to some stimulus, operating near equilibrium (and at high enzyme level) is a good strategy: a small change in reactant concentrations can reverse the reaction direction while maintaining a similar absolute flux. This may be particularly important for glycolysis, where some carbon sources require glycolytic flux (*e.g.*, glucose and fructose) and others require flux in the direction of gluconeogenesis (*e.g.*, acetate and succinate). Therefore, fast environmental fluctuations in the availability of carbon sources may require speedy reversal of most glycolytic reactions, which is consistent with recent measurements indicating that reactions in glycolysis mostly operate with low driving-force in *E. coli* [45,96]. Other functional advantages of working near equilibrium were recently suggested [97,98].

Our methodology takes into account the physiological conditions, including pH, ionic strength, metabolite concentration ranges and cofactor concentrations. This feature is useful when comparing different organisms hosting the same pathway in different conditions. At the same time, the exact values of some of these parameters are not known with high certainty. In particular, the definition of the metabolite concentration range used in the optimization is challenging, as especially high (>10 mM) and especially low (<1 μM) metabolite concentrations have been measured (*e.g.*, [45]). Furthermore, the physicochemical properties of the metabolites affect their cellular concentrations [44], suggesting that the concentration ranges should be individually tailored to each metabolite.

It is important to remember that the MDF methodology assumes that metabolite concentrations are optimized to achieve the most favorable thermodynamics. These optima are calculated using thermodynamic and stoichiometric data with respect to a single pathway and ignoring the rest of the endogenous metabolic network. Yet, *in-vivo* metabolite concentrations are constrained by

many other factors, including their stability, permeability and their participation in other metabolic routes, and so cellular concentrations are unlikely to match these optima precisely. Hence, many of the pathways we analyzed might be more thermodynamically constrained than suggested by the MDF analysis

Our analysis is sensitive to the definition of reactions, *i.e.*, what counts as independent metabolic steps. Merging reactions into a single metabolic step or splitting them into several steps can considerably affect the MDF of a pathway and the Flux-Force Efficacies of its reactions. For example, consider a reaction dissipating 2 kJ/mol and hence operating at a Flux-Force Efficacy of ≈40%. If this reaction is split into two steps, each of these will optimally dissipate 1 kJ/mol and its Flux-Force Efficacy will be only ≈20%. Hence, dividing a pathway into more steps results in lower MDF and Flux-Force Efficacies. Yet, the definition of metabolic steps is not arbitrary. A reaction should be treated as an independent metabolic step if all of its substrates and products are soluble. On the other hand, if two reactions involve a common reactant which remains bound to the enzyme(s), they can be treated as a single metabolic step [9,74], as was suggested for channeling of oxaloacetate between malate dehydrogenase and citrate synthase.

Notably, the MDF analysis is insensitive to the kinetic parameters of the enzymes participating in the pathway. In reality, the net reaction flux is determined both by the internal and external reaction energetics. Internal reaction energetics refers to the thermodynamic landscape associated with (i) the binding and release of the reactants from the enzyme's active site; (ii) the different reaction intermediates formed during catalysis; and (iii) the activation energies of converting one reaction intermediate to another [99]. The internal reaction energetics determines the apparent kinetic parameters of the enzyme catalyzing the reaction (*i.e.*, k_{cat}, K_M) [99]. On the other hand, the external reaction energetics refers to the driving force of the net reaction, which depends on the concentrations of the substrates and products, as analyzed in this manuscript. Figure 4 schematically demonstrates the interplay between the net reaction flux and the internal and external energetic profiles. A reaction with a low k_{cat}/K_M should be compensated by a high driving force (Figure 4A), because otherwise the net flux will be low (Figure 4B). On the other hand, a reaction having a high k_{cat}/K_M can operate closer to equilibrium (*i.e.*, at a low driving force) and still sustain a high net flux (Figure 4C). Finally, a high driving force and a low internal thermodynamic barrier result in a very high net flux (Figure 4D).

Interestingly, the thermodynamic driving forces of reactions can be directly connected to their control coefficients [27,30,100, 101,102]: for a reaction that has a low thermodynamic driving force, the forward and backward fluxes are considerably larger than the net flux. For a near-equilibrium reaction, then, increasing the enzyme concentration will increase the forward and reverse fluxes to a comparable degree, bringing reactant concentrations even closer to equilibrium. This, in turn, lowers the already-low driving force of the reaction and neutralizes the effect of increasing the enzyme concentration. In brief, increasing the abundance of an enzyme catalyzing a near-equilibrium reaction will have only a modest effect on pathway flux.

On the other hand, a reaction with a high driving force will exert high control on the pathway flux. For such a reaction the net flux roughly equals the forward flux, which is much larger than the reverse flux. In this case, increasing the enzyme abundance will mostly increase the forward flux (in absolute terms). Even if the driving force decreases somewhat, the flux-force efficacy will remain high (see Fig. 1A). Hence, an increase in enzyme abundance will not be compensated and will have a considerable

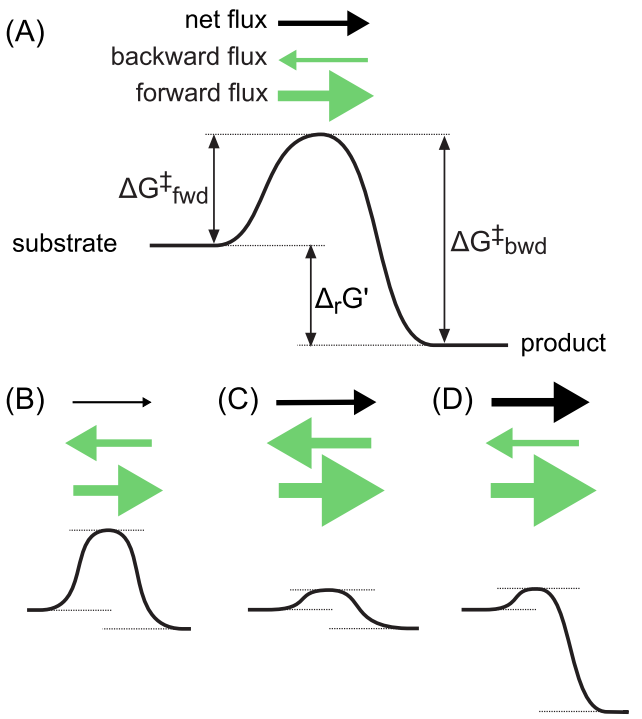

Figure 4. Schematic representation of the interplay between the net reaction flux and the internal and external (i.e., overall or net) energetic profiles. Δ_rG' corresponds to the driving force of the net reaction (which depends on the concentrations of the substrates and products); $\Delta G^{\ddagger}_{fwd}$ to the thermodynamic barrier of the forward reaction, associated with the binding of the substrates and with the different reaction intermediates formed during catalysis; and $\Delta G^{\ddagger}_{bwd}$ corresponds to the thermodynamic barrier of the backward reaction, associated with the different reaction intermediates formed during catalysis and with the release of the products. All reactions are assumed to be catalyzed by the same amount of enzyme units. (A) High internal thermodynamic barrier and high thermodynamic driving force. (B) High internal thermodynamic barrier and low thermodynamic driving force. (C) Low internal thermodynamic barrier and low thermodynamic driving force. (D) Low internal thermodynamic barrier and high thermodynamic driving force.
doi:10.1371/journal.pcbi.1003483.g004

effect on reaction rate. In the Methods and Text S1, we detail the direct mathematical relationship between reaction driving forces and flux control coefficients, which shows that upregulation of enzymes catalyzing reactions with high driving force has a large effect on pathway flux.

Our ultimate goal is to establish a single framework that integrates pathway thermodynamics and enzyme kinetics. We believe it should be possible to reformulate measured kinetic data as thermodynamic potentials and analyze pathways in purely energetic terms. By considering the chemical potential of reaction intermediates and integrating these data with the concentrations of soluble pathway intermediates, one can arrive at a more complete analysis of pathway activity. It remains for future research to develop such an integrated framework.

Supporting Information

Figure S1 Structure of oxidative pathways. (A) The ubiquitous TCA cycle. (B) The PEP-glyoxylate pathway which was found to operate in *E. coli* under glucose starvation. (C) A pathway used by *Pseudomonas fluorescens* under conditions of aluminum toxicity. (D) The oxidative pentose-phosphate cycle, which can be used to

fully oxidize sugars into CO2, thus providing NADPH for cellular activity. The reactions marked in red are those with positive shadow prices (at pH 7.5 and ionic strength of 0.2 M). Non-cofactor metabolites shaded in green show positive shadow prices.
(EPS)

Figure S2 Structure of fermentation pathways. (A) Entner-Meyerhof-Parnas (EMP) glycolysis. Blue arrows correspond to the pyruvate formate lyase shunt. Magenta arrows correspond to a bypass of substrate-level phosphorylation. (B) Entner-Doudoroff (ED) glycolysis. (C) Semi-phosphorylative ED glycolysis, as known to operate in some hyperthermophilic archaea. (D) Non-phosphorylative ED glycolysis, as known to operate in some hyperthermophilic archaea. (E) The methylglyoxal pathway, in which dihydroxyacetone phosphate is converted into the highly reactive compound methylglyoxal when the concentration of inorganic phosphate becomes limiting. (F) The suggested phosphoketolase pathway, which uses the pentose phosphate pathway in conjunction with the enzyme phosphoketolase that cleaves xylulose-phosphate to glyceraldehyde-phosphate and acetyl-phosphate. The reactions marked in red are those with positive shadow prices (at pH 7.5 and ionic strength of 0.2 M). Non-cofactor metabolites shaded in green show positive shadow prices.
(EPS)

Text S1 A mathematical derivation and characteristics of the Max-min Driving Force and its relation to Metabolic Control Analysis.
(PDF)

Acknowledgments

We would like to thank Dan Tawfik and Adrian Jinich for helpful discussions and critical reading of the manuscript.

Author Contributions

Conceived and designed the experiments: EN ABE AF RM. Performed the experiments: EN ABE AF. Analyzed the data: EN ABE WL. Contributed reagents/materials/analysis tools: EN ER WL. Wrote the paper: EN ABE AF ER WL RM.

References

1. Heinrich R, Montero F, Klipp E, Waddell TG, Melendez-Hevia E (1997) Theoretical approaches to the evolutionary optimization of glycolysis: thermodynamic and kinetic constraints. Eur J Biochem 243: 191–201.
2. Melendez-Hevia E, Waddell TG, Heinrich R, Montero F (1997) Theoretical approaches to the evolutionary optimization of glycolysis–chemical analysis. Eur J Biochem 244: 527–543.
3. Stephani A, Nuno JC, Heinrich R (1999) Optimal stoichiometric designs of ATP-producing systems as determined by an evolutionary algorithm. J Theor Biol 199: 45–61.
4. Ebenhoh O, Heinrich R (2001) Evolutionary optimization of metabolic pathways. Theoretical reconstruction of the stoichiometry of ATP and NADH producing systems. Bull Math Biol 63: 21–55.
5. Segre D, Vitkup D, Church GM (2002) Analysis of optimality in natural and perturbed metabolic networks. Proc Natl Acad Sci U S A 99: 15112–15117.
6. Schuster S, Pfeiffer T, Fell DA (2008) Is maximization of molar yield in metabolic networks favoured by evolution? J Theor Biol 252: 497–504.
7. Molenaar D, van Berlo R, de Ridder D, Teusink B (2009) Shifts in growth strategies reflect tradeoffs in cellular economics. Mol Syst Biol 5: 323.
8. Noor E, Eden E, Milo R, Alon U (2010) Central carbon metabolism as a minimal biochemical walk between precursors for biomass and energy. Mol Cell 39: 809–820.
9. Bar-Even A, Flamholz A, Noor E, Milo R (2012) Thermodynamic constraints shape the structure of carbon fixation pathways. Biochim Biophys Acta 1817: 1646–1659.
10. Bar-Even A, Flamholz A, Noor E, Milo R (2012) Rethinking glycolysis: on the biochemical logic of metabolic pathways. Nat Chem Biol 8: 509–517.
11. Bar-Even A, Noor E, Milo R (2012) A survey of carbon fixation pathways through a quantitative lens. J Exp Bot 63: 2325–2342.
12. Schuetz R, Zamboni N, Zampieri M, Heinemann M, Sauer U (2012) Multidimensional optimality of microbial metabolism. Science 336: 601–604.
13. Flamholz A, Noor E, Bar-Even A, Liebermeister W, Milo R (2013) Glycolytic strategy as a tradeoff between energy yield and protein cost. Proc Natl Acad Sci U S A 110: 10039–10044.
14. Bar-Even A, Noor E, Lewis NE, Milo R (2010) Design and analysis of synthetic carbon fixation pathways. Proc Natl Acad Sci U S A 107: 8889–8894.
15. Vojinovic V, von Stockar U (2009) Influence of uncertainties in pH, pMg, activity coefficients, metabolite concentrations, and other factors on the analysis of the thermodynamic feasibility of metabolic pathways. Biotechnol Bioeng 103: 780–795.
16. von Stockar U, Maskow T, Liu J, Marison IW, Patino R (2006) Thermodynamics of microbial growth and metabolism: an analysis of the current situation. J Biotechnol 121: 517–533.
17. Hatzimanikatis V, Li C, Ionita JA, Henry CS, Jankowski MD, et al. (2005) Exploring the diversity of complex metabolic networks. Bioinformatics 21: 1603–1609.
18. Finley SD, Broadbelt LJ, Hatzimanikatis V (2009) Thermodynamic analysis of biodegradation pathways. Biotechnol Bioeng 103: 532–541.
19. Miskovic L, Hatzimanikatis V (2010) Production of biofuels and biochemicals: in need of an ORACLE. Trends Biotechnol 28: 391–397.
20. Bar-Even A, Noor E, Flamholz A, Milo R (2013) Design and analysis of metabolic pathways supporting formatotrophic growth for electricity-dependent cultivation of microbes. Biochim Biophys Acta 1827: 1039–1047.
21. Beard DA, Qian H (2005) Thermodynamic-based computational profiling of cellular regulatory control in hepatocyte metabolism. Am J Physiol Endocrinol Metab 288: E633–644.
22. Noor E, Bar-Even A, Flamholz A, Lubling Y, Davidi D, et al. (2012) An integrated open framework for thermodynamics of reactions that combines accuracy and coverage. Bioinformatics 28: 2037–2044.
23. Beard DA, Qian H (2007) Relationship between thermodynamic driving force and one-way fluxes in reversible processes. PLoS One 2: e144.
24. Rottenberg H (1973) The thermodynamic description of enzyme-catalyzed reactions. The linear relation between the reaction rate and the affinity. Biophys J 13: 503–511.
25. Van Der Meer R, Westerhoff HV, Van Dam K (1980) Linear relation between rate and thermodynamic force in enzyme-catalyzed reactions. Biochim Biophys Acta 591: 488–493.
26. Kacser H, Burns JA (1973) The control of flux. Symp Soc Exp Biol 27: 65–104.
27. Westerhoff HV (1987) Thermodynamics and Control of Biological Free-Energy Transduction: Elsevier Science Ltd.
28. Acerenza L (1993) Metabolic control design. J Theor Biol 165: 63–85.
29. Crabtree B, Newsholme EA, Reppas NB (1997) Principles of regulation and control in biochemistry: a pragmatic, flux-oriented approach. In: Hoffman JF, Jamieson JD, editors. Handbook of Physiology. New York, USA: Oxford University Press.pp. 117–180.
30. Nielsen J (1997) Metabolic control analysis of biochemical pathways based on a thermokinetic description of reaction rates. Biochem J 321 (Pt 1): 133–138.
31. Bar-Even A, Noor E, Savir Y, Liebermeister W, Davidi D, et al. (2011) The moderately efficient enzyme: evolutionary and physicochemical trends shaping enzyme parameters. Biochemistry 50: 4402–4410.
32. Noor E, Haraldsdottir HS, Milo R, Fleming RMT (2013) Consistent estimation of GIbbs energy using component contributions. Plos Comp Biol: 9: e1003098.
33. Alberty RA (2003) Thermodynamics of Biochemical Reactions: Wiley-Interscience.
34. Alberty RA (2006) Biochemical thermodynamics: applications of Mathematica. Methods Biochem Anal 48: 1–458.
35. Goldberg RN, Tewari YB, Bhat TN (2004) Thermodynamics of enzyme-catalyzed reactions–a database for quantitative biochemistry. Bioinformatics 20: 2874–2877.
36. Goldberg RN, Tewari YB, Bhat TN (2007) Thermodynamics of enzyme-catalyzed reactions: Part 7—2007 update J Phys Chem Ref Data 36: 1347–1397.
37. Slonczewski JL, Fujisawa M, Dopson M, Krulwich TA (2009) Cytoplasmic pH measurement and homeostasis in bacteria and archaea. Adv Microb Physiol 55: 1–79, 317.
38. McNaught AD, Wilkinson A (1997) Compendium of Chemical Terminology, 2nd ed. (the IUPAC "Gold Book"). Oxford: Blackwell Scientific Publications.
39. Alberty RA (1996) Calculation of biochemical net reactions and pathways by using matrix operations. Biophys J 71: 507–515.
40. Brochado AR, Andrejev S, Maranas CD, Patil KR (2012) Impact of stoichiometry representation on simulation of genotype-phenotype relationships in metabolic networks. PLoS Comput Biol 8: e1002758.
41. Mavrovouniotis ML (1993) Identification of localized and distributed bottlenecks in metabolic pathways. Proc Int Conf Intell Syst Mol Biol 1: 275–283.

42. Kelly FP, Maulloo AK, Tan DKH (1998) Rate control for communication networks: shadow prices, proportional fairness and stability. J Oper Res Soc 49: 237–252.
43. Bertsimas D, Tsitsiklis JN, Tsitsiklis J (1997) Introduction to Linear Optimization.
44. Bar-Even A, Noor E, Flamholz A, Buescher JM, Milo R (2011) Hydrophobicity and charge shape cellular metabolite concentrations. PLoS Comput Biol 7: e1002166.
45. Bennett BD, Kimball EH, Gao M, Osterhout R, Van Dien SJ, et al. (2009) Absolute metabolite concentrations and implied enzyme active site occupancy in Escherichia coli. Nat Chem Biol 5: 593–599.
46. Zampar GG, Kummel A, Ewald J, Jol S, Niebel B, et al. (2013) Temporal system-level organization of the switch from glycolytic to gluconeogenic operation in yeast. Mol Syst Biol 9: 651.
47. Ugurbil K, Rottenberg H, Glynn P, Shulman RG (1982) Phosphorus-31 nuclear magnetic resonance studies of bioenergetics in wild-type and adenosinetriphosphatase(1-) Escherichia coli cells. Biochemistry 21: 1068–1075.
48. Koebmann BJ, Westerhoff HV, Snoep JL, Nilsson D, Jensen PR (2002) The glycolytic flux in Escherichia coli is controlled by the demand for ATP. J Bacteriol 184: 3909–3916.
49. Ishii N, Nakahigashi K, Baba T, Robert M, Soga T, et al. (2007) Multiple high-throughput analyses monitor the response of E. coli to perturbations. Science 316: 593–597.
50. de Graef MR, Alexeeva S, Snoep JL, Teixeira de Mattos MJ (1999) The steady-state internal redox state (NADH/NAD) reflects the external redox state and is correlated with catabolic adaptation in Escherichia coli. J Bacteriol 181: 2351–2357.
51. Bautista J, Satrustegui J, Machado A (1979) Evidence suggesting that the NADPH/NADP ratio modulates the splitting of the isocitrate flux between the glyoxylic and tricarboxylic acid cycles, in Escherichia coli. FEBS Lett 105: 333–336.
52. Stiefel EI, George GN (1994) Ferredoxins, Hydrogenases, and Nitrogenases: Metal-Sulfide Proteins. Bioinorganic Chemistry. pp. 365–453.
53. Ugurbil K, Rottenberg H, Glynn P, Shulman RG (1978) 31P nuclear magnetic resonance studies of bioenergetics and glycolysis in anaerobic Escherichia coli cells. Proc Natl Acad Sci U S A 75: 2244–2248.
54. Xavier KB, Kossmann M, Santos H, Boos W (1995) Kinetic analysis by in vivo 31P nuclear magnetic resonance of internal Pi during the uptake of sn-glycerol-3-phosphate by the pho regulon-dependent Ugp system and the glp regulon-dependent GlpT system. J Bacteriol 177: 699–704.
55. Moreau PL, Gerard F, Lutz NW, Cozzone P (2001) Non-growing Escherichia coli cells starved for glucose or phosphate use different mechanisms to survive oxidative stress. Mol Microbiol 39: 1048–1060.
56. Chen J, Brevet A, Fromant M, Leveque F, Schmitter JM, et al. (1990) Pyrophosphatase is essential for growth of Escherichia coli. J Bacteriol 172: 5686–5689.
57. Stockbridge RB, Wolfenden R (2011) Enhancement of the rate of pyrophosphate hydrolysis by nonenzymatic catalysts and by inorganic pyrophosphatase. J Biol Chem 286: 18538–18546.
58. Fell D (1996) Understanding the Control of Metabolism: Portland Pr.
59. Klipp E, Liebermeister W, Wierling C, Kowald A, Lehrach H, et al. (2009) Systems Biology: Wiley-Blackwell.
60. Haldane JBS (1930) Enzymes. London: Longmans & Green.
61. Noor E, Flamholz A, Liebermeister W, Bar-Even A, Milo R (2013) A note on the kinetics of enzyme action: A decomposition that highlights thermodynamic effects. FEBS Lett 587: 2772–2777.
62. O'Boyle NM, Banck M, James CA, Morley C, Vandermeersch T, et al. (2011) Open Babel: An open chemical toolbox. J Cheminform 3: 33.
63. Kanehisa M, Araki M, Goto S, Hattori M, Hirakawa M, et al. (2008) KEGG for linking genomes to life and the environment. Nucleic Acids Res 36: D480–484.
64. Fischer E, Sauer U (2003) A novel metabolic cycle catalyzes glucose oxidation and anaplerosis in hungry Escherichia coli. J Biol Chem 278: 46446–46451.
65. Chen X, Alonso AP, Allen DK, Reed JL, Shachar-Hill Y (2011) Synergy between (13)C-metabolic flux analysis and flux balance analysis for understanding metabolic adaptation to anaerobiosis in E. coli. Metab Eng 13: 38–48.
66. Wright BE, Butler MH, Albe KR (1992) Systems analysis of the tricarboxylic acid cycle in Dictyostelium discoideum. I. The basis for model construction. J Biol Chem 267: 3101–3105.
67. Ringe D, Petsko GA (2008) Biochemistry. How enzymes work. Science 320: 1428–1429.
68. Weber AL (2004) Kinetics of organic transformations under mild aqueous conditions: implications for the origin of life and its metabolism. Orig Life Evol Biosph 34: 473–495.
69. Pharkya P, Nikolaev EV, Maranas CD (2003) Review of the BRENDA Database. Metab Eng 5: 71–73.
70. Datta A, Merz JM, Spivey HO (1985) Substrate channeling of oxalacetate in solid-state complexes of malate dehydrogenase and citrate synthase. J Biol Chem 260: 15008–15012.
71. Tompa P, Batke J, Ovadi J, Welch GR, Srere PA (1987) Quantitation of the interaction between citrate synthase and malate dehydrogenase. J Biol Chem 262: 6089–6092.
72. Srere PA (1987) Complexes of sequential metabolic enzymes. Annu Rev Biochem 56: 89–124.
73. Morgunov I, Srere PA (1998) Interaction between citrate synthase and malate dehydrogenase. Substrate channeling of oxaloacetate. J Biol Chem 273: 29540–29544.
74. Bar-Even A (2013) Does acetogenesis really require especially low reduction potential? Biochim Biophys Acta 1827: 395–400.
75. van der Rest ME, Frank C, Molenaar D (2000) Functions of the membrane-associated and cytoplasmic malate dehydrogenases in the citric acid cycle of Escherichia coli. J Bacteriol 182: 6892–6899.
76. Kather B, Stingl K, van der Rest ME, Altendorf K, Molenaar D (2000) Another unusual type of citric acid cycle enzyme in Helicobacter pylori: the malate:quinone oxidoreductase. J Bacteriol 182: 3204–3209.
77. Molenaar D, van der Rest ME, Drysch A, Yucel R (2000) Functions of the membrane-associated and cytoplasmic malate dehydrogenases in the citric acid cycle of Corynebacterium glutamicum. J Bacteriol 182: 6884–6891.
78. Dufresne A, Salanoubat M, Partensky F, Artiguenave F, Axmann IM, et al. (2003) Genome sequence of the cyanobacterium Prochlorococcus marinus SS120, a nearly minimal oxyphototrophic genome. Proc Natl Acad Sci U S A 100: 10020–10025.
79. Forster-Fromme K, Jendrossek D (2005) Malate:quinone oxidoreductase (MqoB) is required for growth on acetate and linear terpenes in Pseudomonas citronellolis. FEMS Microbiol Lett 246: 25–31.
80. Sweetlove LJ, Beard KF, Nunes-Nesi A, Fernie AR, Ratcliffe RG (2010) Not just a circle: flux modes in the plant TCA cycle. Trends Plant Sci 15: 462–470.
81. Singh R, Lemire J, Mailloux RJ, Chenier D, Hamel R, et al. (2009) An ATP and oxalate generating variant tricarboxylic acid cycle counters aluminum toxicity in Pseudomonas fluorescens. PLoS One 4: e7344.
82. Noguchi Y, Nakai Y, Shimba N, Toyosaki H, Kawahara Y, et al. (2004) The energetic conversion competence of Escherichia coli during aerobic respiration studied by 31P NMR using a circulating fermentation system. J Biochem 136: 509–515.
83. Sung SJS, Xu DP, Galloway CM, Black CCJ (1988) A reassessment of glycolysis and gluconeogenesis in higher plants. Physiol Plant 72: 650–654.
84. Verhees CH, Kengen SW, Tuininga JE, Schut GJ, Adams MW, et al. (2003) The unique features of glycolytic pathways in Archaea. Biochem J 375: 231–246.
85. Kalapos MP (1999) Methylglyoxal in living organisms: chemistry, biochemistry, toxicology and biological implications. Toxicol Lett 110: 145–175.
86. Zhang X, Harrison DH, Cui Q (2002) Functional specificities of methylglyoxal synthase and triosephosphate isomerase: a combined QM/MM analysis. J Am Chem Soc 124: 14871–14878.
87. Hopper DJ, Cooper RA (1971) The regulation of Escherichia coli methylglyoxal synthase; a new control site in glycolysis? FEBS Lett 13: 213–216.
88. Siebers B, Schonheit P (2005) Unusual pathways and enzymes of central carbohydrate metabolism in Archaea. Curr Opin Microbiol 8: 695–705.
89. Ahmed H, Ettema TJ, Tjaden B, Geerling AC, van der Oost J, et al. (2005) The semi-phosphorylative Entner-Doudoroff pathway in hyperthermophilic archaea: a re-evaluation. Biochem J 390: 529–540.
90. Sonderegger M, Schumperli M, Sauer U (2004) Metabolic engineering of a phosphoketolase pathway for pentose catabolism in Saccharomyces cerevisiae. Appl Environ Microbiol 70: 2892–2897.
91. Bogorad IW, Lin TS, Liao JC (2013) Synthetic non-oxidative glycolysis enables complete carbon conservation. Nature.
92. Noor E, Milo R (2012) Evolution. Efficiency in evolutionary trade-offs. Science 336: 1114–1115.
93. Alexeeva S, de Kort B, Sawers G, Hellingwerf KJ, de Mattos MJ (2000) Effects of limited aeration and of the ArcAB system on intermediary pyruvate catabolism in Escherichia coli. J Bacteriol 182: 4934–4940.
94. Levanon SS, San KY, Bennett GN (2005) Effect of oxygen on the Escherichia coli ArcA and FNR regulation systems and metabolic responses. Biotechnol Bioeng 89: 556–564.
95. Zhu J, Shalel-Levanon S, Bennett G, San KY (2007) The YfiD protein contributes to the pyruvate formate-lyase flux in an Escherichia coli arcA mutant strain. Biotechnol Bioeng 97: 138–143.
96. Link H, Kochanowski K, Sauer U (2013) Systematic identification of allosteric protein-metabolite interactions that control enzyme activity in vivo. Nat Biotechnol 31: 357–361.
97. Ruzanski C, Smirnova J, Rejzek M, Cockburn D, Pedersen HL, et al. (2013) A bacterial glucanotransferase can replace the complex maltose metabolism required for starch to sucrose conversion in leaves at night. J Biol Chem 288: 28581–28598.
98. Kartal O, Mahlow S, Skupin A, Ebenhoh O (2011) Carbohydrate-active enzymes exemplify entropic principles in metabolism. Mol Syst Biol 7: 542.
99. Fersht A (1998) Structure and Mechanism in Protein Science: A Guide to Enzyme Catalysis and Protein Folding. New York: W. H. Freeman.
100. Visser D, Schmid JW, Mauch K, Reuss M, Heijnen JJ (2004) Optimal re-design of primary metabolism in Escherichia coli using linlog kinetics. Metab Eng 6: 378–390.
101. Wang L, Birol I, Hatzimanikatis V (2004) Metabolic control analysis under uncertainty: framework development and case studies. Biophys J 87: 3750–3763.

102. Kummel A, Panke S, Heinemann M (2006) Putative regulatory sites unraveled by network-embedded thermodynamic analysis of metabolome data. Mol Syst Biol 2 : 2006 0034.

103. Schramm M, Klybas V, Racker E (1958) Phosphorolytic cleavage of fructose-6-phosphate by fructose-6-phosphate phosphoketolase from Acetobacter xylinum. J Biol Chem 233: 1283–1288.